On the feasibility of using a laser guide star adaptive optics system in the daytime

Ryan Dungee
Mark Chun
Yutaka Hayano

On the feasibility of using a laser guide star adaptive optics system in the daytime

Ryan Dungee,[a,*] Mark Chun,[b] and Yutaka Hayano[c]
[a]University of Hawaii, Institute for Astronomy, Honolulu, Hawaii, United States
[b]University of Hawaii, Institute for Astronomy, Hilo, Hawaii, United States
[c]National Astronomical Observatory of Japan, Tokyo, Japan

Abstract. We investigate the use of ultra-narrow band interference filters to enable daytime use of sodium laser guide star (LGS) adaptive optics systems. Filter performance is explored using theoretical and vendor supplied filter transmission profiles, a modeled daylight sky background, broadband measurements of the daytime sky brightness on Maunakea, and an assumed photon return from the sodium LGS and read noise for the wavefront sensor (WFS) detector. The critical parameters are the bandpass of the filter, the out-of-band rejection, and the peak throughput at the wavelength of the LGS light. Importantly, a systematic trade between these parameters leads to potentially simple solutions enabling daytime observations. Finally, we simulated the Mid-Infrared Adaptive Optics (MIRAO) system planned for the Thirty Meter Telescope with an end-to-end simulation, folding in daytime sky counts. We find that MIRAO with five sodium LGSs, commercial off-the-shelf filters to suppress the sky background in the LGS WFSs, and a near-infrared natural guide star ($K \leq 13$) tip/tilt/focus WFS can attain daytime Strehl ratio values comparable to those at night. © *The Authors. Published by SPIE under a Creative Commons Attribution 4.0 Unported License. Distribution or reproduction of this work in whole or in part requires full attribution of the original publication, including its DOI.* [DOI: 10.1117/1.JATIS.5.1.019002]

Keywords: adaptive optics; laser guide star; daylight observing; wavefront sensing.

Paper 18071 received Sep. 4, 2018; accepted for publication Dec. 26, 2018; published online Jan. 25, 2019.

1 Introduction

At wavelengths longward of $\sim 2~\mu m$, the sky background in ground-based observations begins to be dominated by the thermal emission of the telescope and the atmosphere.[1] Around $\sim 3~\mu m$, this thermal background is so strong that the sky background does not change appreciably between the night and the day. As a result, ground-based observatories can perform mid-infrared (mid-IR) observations during the day with little impact on the sensitivity of the observation.[1] Some facilities, such as the NASA Infrared Telescope Facility (IRTF), routinely make observations during the day as a way of extending the science time available to their users. This practice is not common as there are a few extra complications associated with operating during the day. Nonetheless, early morning hours which are no longer suitable for optical observations can be used for IR observing to extend the operation time of a telescope with little to no additional engineering. Even an hour of additional time during the morning twilight would increase the total telescope time available for science observations by $\sim 10\%$. Given the construction and operating costs of the current and next generation of large ground-based telescopes, such an increase in time is extremely valuable.

However, for the next generation of extremely large telescopes, there is a secondary consideration since they require adaptive optics (AO) systems at mid-IR wavelengths to reach the diffraction limit.[1] The Thirty Meter Telescope (TMT), one of the next generation ground-based telescopes, is being designed with AO as an integral part of the facility. The first-light AO system (NFIRAOS),[2,3] optimized for observations at near-IR wavelengths, will use a sodium laser guide star

(LGS) system in order to maximize the area of sky, where they can obtain diffraction-limited observations. The wavelength of the D_2 transition in sodium, 589.0 nm, falls well within the visible range meaning the return signal from the LGS would normally be drowned out by the daytime sky. However, the spectral bandwidth of the sodium LGS return light is on the order of a few picometers, so, in principle, a sufficiently narrow spectral bandpass filter can be used to isolate the LGS light from the sky background.

Beckers and Cacciani[1] proposed the use of a sodium LGS system during the daytime with applications in both solar astronomy and in the mid-IR. Beckers revisited these ideas in 2008 laying out both site-specific considerations and the use of such mid-IR instruments in the era of James Webb Space Telescope.[4] Hart et al.[5] performed the first measurement of the achievable contrast between an LGS and the daytime sky. For this experiment, Hart et al. used a magneto-optical filter (MOF), as suggested by Beckers and Cacciani. An MOF uses sodium vapor surrounded by a strong magnetic field to rotate the polarization of light resonant with transitions in the sodium. By using crossed linear polarizers at the front and rear of the sodium cell and a vapor temperature/magnetic field configuration that rotates the polarization of the resonant light by 90 deg. All wavelengths not interacting with the magnetized sodium atoms are attenuated at the level of the crossed polarizers ($\sim 10^6$). This allows the filter to attain extremely narrow bandwidths.

However, the MOF approach carries with it a number of disadvantages: (1) it is a large bulky device, (2) it requires a heated sodium cell, and (3) the overall throughput is low. The use of a such a filter within a wavefront sensor (WFS) will require substantial engineering to fit it into the WFS and to mitigate any localized turbulence created by the sodium vapor, which has temperatures ranging from $150^{\circ}C$ to $200^{\circ}C$.

*Address all correspondence to Ryan Dungee, E-mail: rdungee@hawaii.edu

In order to address these disadvantages, we explored (1) the trade-offs between different sodium line filter specifications and their impact on the signal-to-noise ratio (SNR) of the WFS measurements and (2) how this SNR translates into AO performance using detailed simulations of the full system. In the rest of this paper, we discuss the results of our filter specification trade study (Sec. 2), the AO performance simulations (Sec. 3), discuss particular concerns and implications of the proposed approach (Sec. 4), and present our conclusions on the feasibility of daytime LGS AO (Sec. 5).

2 Filter Requirements

There are many sources of error that impact the performance of an AO system. For this work, the pertinent sources of error are encapsulated in the WFS measurement error. Here, we consider a Shack–Hartmann WFS (SHWFS) as it is the most common type of WFS in use with sodium LGSs. In a SHWFS, the wavefront gradient measurement error is proportional to the surface brightness and subaperture spot size, and inversely proportional to the SNR.[6] In this work, we make the assumption that the WFS spot size is independent of the approach we take to filtering the sky background and as such we focus on the changes to SNR. The SNR depends on a wide range of parameters (see Table 1), many of which can be tuned throughout the AO design process. As a first step, we assumed a fixed AO system and focused only on the parameters, which a filter could directly affect. These SNR values are calculated using a standard formula, where the terms and their assumed values are defined in Table 1:

$$\text{SNR} = \frac{S}{\sqrt{S + B + n_{\text{pix}}RN^2}}. \tag{1}$$

The signal S is derived from the TMT specification for the sodium LGS return for NFIRAOS and corresponds to an LGS magnitude of $R \approx 8.2$, a value routinely achieved by Keck II.[9] For this initial trade study on filter requirements, S depends only on the transmission of the filter at 589.0 nm (T_{589}). We based this on the assumption that we would not choose a filter with a bandpass narrower than that of the laser return light, and thus, the peak transmission of the filter is the only aspect which would block the laser return. The background B is calculated from an integral over the product of our model sky spectrum (Sec. 2.1)

and selected filter transmission profile. Finally, the read noise, RN, is derived from the TMT specification for the read noise per pixel for the NFIRAOS WFS cameras and an assumption of the number of pixels covering the subaperture field-of-view (FoV). This sets the read noise at 3 electrons/pixel when operating at a frame rate of 800 Hz. Detector sizes range from 6×6 pixels to 6×16 pixels depending on the LGS's elongation in the subaperture's FoV. Recent tests of detectors for the TMT WFSs have achieved a read noise between 3 and 3.5 electrons.[8] However, we note that given the bright, daytime sky background, we are not read noise limited and, as our later discussions will demonstrate (Sec. 3), the achieved range of read noise values are well within an acceptable range.

2.1 On-Sky Tests

Our model sky spectrum is derived from broadband measurements of the daytime sky and a solar spectrum provided by the Harvard-Smithsonian Center for Astrophysics[10] modified to have a Rayleigh scattering wavelength dependence of λ^{-4}. In the visible band, we obtained measurements for Johnson V, and Sloan g, r, i, and z broadband filters from the MORIS instrument on IRTF.[11] Photometric calibrations for the instrument were obtained from previous observations of a standard star. Observations were of a patch of clear sky 90 deg away from the sun ~3 h after sunrise. The results of these observations are summarized in Table 2.

Table 2 Measured sky brightnesses at an elevation of ~60 deg and ~3 h after sunrise.

Filter name	Magnitude per square arc sec
Sloan g	3.4 ± 0.1
r	4.5 ± 0.1
i	5.2 ± 0.1
z	5.6 ± 0.1
Johnson V	3.9 ± 0.1
MKO K	7.2 ± 0.1

Table 1 Symbols for Eq. (1).

Variable	Description	Definition[a]	Reference for values
S	Signal	$\eta D_{\text{subap}}^2 t T_{589}$[b] 900[c]	Boyer et al.[7]
B	Background	$\eta D_{\text{subap}}^2 t \Delta \lambda$[d] $\Omega_{\text{FOV}} F_{\text{sky}}$	Boyer et al.[7] and Sec. 2.1
n_{pix}	Pixels per subaperture	6×16 pixels[e]	Ellerbroek et al.[8]
RN	RMS detector read noise	$3e^-$	Ellerbroek et al.[8]

[a]All variables in this column are defined relative to their NFIRAOS specifications unless otherwise stated. These specifications call for a total efficiency (η) of 0.42, a subaperture diameter (D_{subap}) of 0.5 m, an integration time (t) of 1/800 s, and a pixel scale (Ω_{FoV}) of 0.5 arc sec.
[b]T_{589} is the transmission of a given filter at 589.0 nm, the specified return wavelength of the LGS.
[c]Photo-detection events per subaperture per frame in the WFS for the Narrow Field Infrared Adaptive Optics System (NFIRAOS).
[d]The term $\Delta\lambda$ is intended to represent the operation of an integral over the product of a narrow-band filter profile with our model sky spectrum.
[e]We always assume the largest detector size to make our estimates conservative.
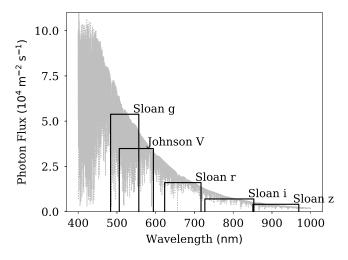
Fig. 1 In gray, the model spectrum we use as input for our SNR calculations. Solid black lines plotted over the spectrum are our measurements (see Table 2), converted from magnitudes into the number of photons our WFS would measure through that filter's passband and binned at the same resolution as the spectrum. For further details, see Sec. 2.1.

We fit the model sky spectrum to the five broadband measurements using the normalization as our only free parameter. The results (see Fig. 1) were checked by comparing broadband counts in our model spectrum to their corresponding measurement, indicating our model spectrum is accurate to ±20%. Overall, our model sky spectrum is conservative with respect to our measurements. Our model's overestimation is readily visualized in Fig. 1, where each measured sky magnitude was converted into an average photon flux for the corresponding passband. This model sky spectrum is used in our sensitivity study (Sec. 2.2) and our simulations (Sec. 3).

Due to the nature of Rayleigh scattering, the surface brightness of the sky may fluctuate as a function of time of day, conditions, and look-angle. None of these effects are captured in our model sky spectrum, however, we refer the reader to Sec. 4.1 for discussion on how these effects impact our results.

2.2 Sensitivity to Filter Parameters

To test the importance of various filter parameters, we performed a sensitivity study by generating a number of theoretical transmission profiles, multiplying them with our model daytime sky spectrum and integrating. Filter traces were generated with different bandwidths, out-of-band rejections, and peak transmission values. Mock filter traces with a bandwidth less than 0.2 nm had a Gaussian profile, whereas filters wider than 0.2 nm had a roughly box profile, with edges that decayed exponentially. Once a profile reaches the smallest transmission value, set by the out-of-band rejection, it switches to a flat profile for the rest of the spectrum. The photon count left after the integration of the product of our profile and model sky spectrum was then used as the background in Eq. (1). The T_{589} value folded into the signal in Eq. (1) was determined by the mock filter's peak transmission. All profiles were assumed to be centered at 589.0 nm and had a minimum transmission specified by the out-of-band rejection given as an optical density (OD).

In varying these three filter parameters, we calculated the SNR of a wide variety of filter transmission profiles. Using an initial performance cut-off of SNR greater than 10, we find that the bandwidth of the filter must be subnanometer to sufficiently block out the sky background but that for bandwidths less than 50 pm the SNR is photon noise limited. Similarly, out-of-band rejections greater than OD~4.5 were found to have diminishing returns. The peak transmission is a critical parameter and it allows the bandwidth of the filter to increase. This is illustrated in Fig. 2, where the 0.5 nm bandpass filter with a high transmission performs nearly as well as the 10 to 50 pm filters with lower transmission. Conversely, a low peak transmission can be compensated by a smaller filter bandpass. However, a peak filter transmission less than about 50% has difficulty achieving the SNR cut-off. Since the SNR in this study is only directly related to the total area under the filter transmission profile, we note that these values are intended to serve as a rough guideline for what values to keep in mind when designing such an AO system. The right-hand panel of Fig. 2 more completely displays the various trades that can be made.
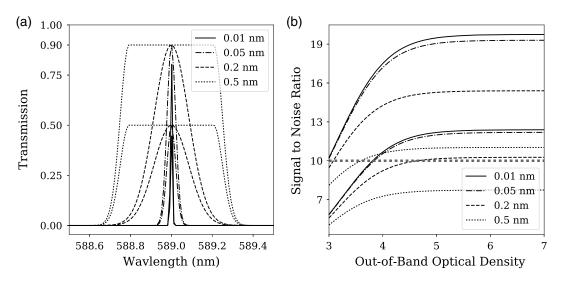

Fig. 2 (a) Examples of the theoretical transmission profiles we used in our sensitivity study, including peak transmissions of 0.5 and 0.9. (b) The out-of-band rejection of the filter expressed as an optical depth versus the SNR. The horizontal dotted line represents our initial cut-off SNR of 10. The AO configuration corresponds to that which is outlined in Table 1, with A of 1.

Table 3 Comparison of various filters.

Filter name	Expected SNR	Bandwidth	Peak transmission	Out-of-band
Alluxa OD4[a]	21.0	0.5 nm	>90%	>OD4
Custom filter A	19.9	~1.0 nm	92.4%	>OD5
Alluxa OD6[b]	16.2	0.8 nm	96.9%	>OD5.7
Keck sodium notch filter	13.8	1.0 nm	90.9%	>OD4
MOF[c]	10.8	~10 pm	<50%[d]	~OD6[e]

[a]The filter's full name is Alluxa 589.16 OD4 ultra narrow.
[b]The filter's full name is Alluxa 589.45 OD6 ultra narrow.
[c]These are estimates based off reported performance from outside sources[5] and private discussions with Wayne Rodgers of Eddy Co. a maker of MOFs.
[d]Return light of the laser is circularly polarized but the MOF construction requires linear polarizers. This value can be boosted by the inclusion of a quarter waveplate.[5]
[e]This depends on the polarizers chosen for the MOF construction.

2.3 Application to Commercial Filters

We obtained transmission profiles for several off-the-shelf and custom filters. Putting these profiles through the same code used in our sensitivity study allowed us to rank their expected performance. The typical resolution provided on a filter's profile was of order 0.06 nm, so to match the resolution of the profiles to our sky spectrum, we used linear interpolation on the provided filter profiles.

The results of these calculations are shown in Table 3. Included in the table are the characteristics of the MOF filter for comparison. Interference filters have the advantage of being a passive optical element with a relatively simple implementation in the AO system. They also typically have much higher peak transmission values. Their principal disadvantage lies in their dependence on the angle of incidence of the beam on the filter, which can lead to a relatively narrow FoV.

Of the interference filters analyzed, the Alluxa 589.16 OD4 Ultra Narrow Bandpass Filter (or "Alluxa OD4") achieved the highest SNR and became the focus of further simulations. As such, much of the following discussion is built around this particular filter's expected performance. Nonetheless, the SNR is a generic enough measure that these discussions can be expected to apply to other filters capable of matching the Alluxa OD4's performance.

The filter profile and FoV for the Alluxa OD4 were measured on the optical bench of the Subaru telescope's sodium laser. Our measurements show that the filter profile is wider than reported by the manufacturer by a factor of ~1.5 the full width at half maximum (FWHM). We have yet to measure the out-of-band rejection but preliminary results from measuring the profile indicate that it reaches the specifications of OD > 4. To measure the filter's profile, we measured throughput as a function of the angle of incidence on the filter and fit the data points with a Gaussian curve to obtain the FWHM, peak transmission, and central wavelength. This yields an estimated FWHM 0.76 nm versus the provided value of 0.5 nm, an estimated peak transmission of 0.94 versus the provided value of 0.96, and an estimated central wavelength of 589.14 nm that agrees with
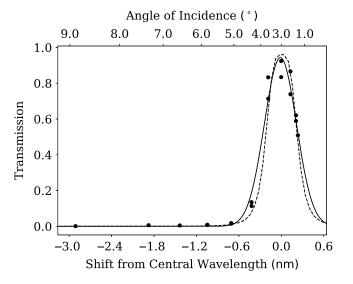

Fig. 3 Filter profiles for the Alluxa OD4 filter. Black dots are measurements, taken in steps of 1 deg by tilting the filter with respect to the laser beam, which is at the wavelength of the sodium D_2 line. The solid black curve is the best fit filter profile assuming a Gaussian curve. The dashed black line is the filter profile provided by Alluxa. Shifts from the central wavelength are computed using the standard approximation $\lambda(\theta) = \lambda_0 \sqrt{\frac{1-x(\theta)}{1-x(-3 \text{ deg})}}$, where $x(\theta) = \frac{\sin \theta}{n_{\text{eff}}}$ where $n_{\text{eff}} = 1.85$ is the effective refractive index[12] for the filter's material and -3 deg is the angle at which transmission through the filter peaked.

the provided value. For a comparison of the measured and provided filter profiles, we refer the reader to Fig. 3.

As with any interference filter, the central wavelength (and by extension the throughput at the wavelength of the sodium D_2 line) varies as a function of the angle of incidence on the filter. This variation with field angle will come into play for WFSs with a small beam size (e.g., large pupil demagnifications). Our measured filter profile shows a throughput greater than 85% for collimated beams with angles of incidence ± 0.7 deg from normal. If we first consider a 10-m telescope with a collimated optical beam size of 10 mm (e.g., a standard one-inch filter) and a subaperture FoV of 2 arc sec, then we have a requirement of ± 0.3 deg. This field propagates through the Alluxa OD4 with little or no field attenuation. However, for next generation large ground-based telescopes such as TMT, the limitation on the FoV will need to be considered due to further elongation of the LGS by the larger aperture and a greater pupil demagnification. We discuss options to address this in Sec. 4.2.

3 Simulations

Since the SNR is not a direct measurement of the AO system's performance, we also ran end-to-end simulations of the TMT MIRAO system. These simulations include the effect of daytime sky on the sodium LGS WFSs as well as the effect of the daytime sky on the low-order (tip/tilt/focus) natural guide star (NGS) WFS that is required with an LGS AO system. They do not include the variation of the filter transmission as a function of field angle. We leave this to a future study.

Simulations are performed using the Multithreaded Adaptive Optics Simulator (MAOS) package.[13] MAOS is an open source Monte-Carlo adaptive optics simulation package created and maintained by the TMT Corporation. The package includes simulation of the wavefront propagating through the atmosphere,

the correction by the deformable mirror, the wavefront sensing by a variety of LGS and NGS WFSs, and the algorithm to reconstruct the wavefront. We add in additional background counts to account for the added sky brightness during the daytime. Since the NGS, in general, has no sufficiently bright spectral feature, the WFS must use a broadband filter preventing a daytime sky suppression analogous to our LGS component. Because of this, we benefit from working at longer wavelengths (e.g., K-band), where the image is partially corrected by the AO system. The image will then have a well corrected diffraction-limited core (~15 mas) allowing us to, in principle, suppress the sky background through a careful selection of the pixel scale and field stop size in the WFS. For this feasibility study, we did not optimize the number of subapertures but rather we sought to demonstrate that there is a stable and useful configuration that enables daytime observing.

3.1 Simulation Setup

For our simulations, the sky backgrounds are calculated and added as a uniform background of photo-detection events per pixel per frame with Poisson noise. Atmospheric conditions are modeled as a set of evolving phase screens in which each add aberrations to the simulated wavefront as it passes through the layer. Each phase screen has a random set of aberrations with a Von Karman spectrum and a wavefront outerscale of 30 m. Given that there is some randomness to each realization, we average the output of 20 independent runs of the simulation. The difference between each independent run is the set of atmospheric screens used. The same 20 sets of atmospheric screens were used for every AO and filter configuration. This allows us to account for variations of the seeing in each realization due to the limited number of simulation steps. We estimate the uncertainty in the resulting mean wavefront error is $(\phi^2)^{+0.02}_{-0.03}$ rad^2, where ϕ^2 is the phase variance of the wavefront or roughly an uncertainty of ±0.01 on the Strehl ratios that we calculated. We determine this estimate from the variance of the mean wavefront error as a function of the number of realizations binned together compared to the averaged output of a set of 70 simulation runs. For characterizing the daytime AO system, we ran batches of simulations for two separate atmospheric conditions, the 50th and 75th percentile seeing cases for Maunakea at 13N. These conditions are based on the TMT site testing campaign[14] and represent median conditions and worse than average night time conditions. We note that we expect daytime observing with sodium LGSs on TMT would be limited to the early morning. During this time, there is evidence that the seeing is very similar to the end of the night values for about 1 to 2 h.[15]

3.2 Stable AO Performance

We split the performance calculations into two steps: identifying a configuration of the high-order LGS WFSs that provided good correction in the mid-IR during the day and the determination of a limiting magnitude for the NGS WFS, which measures tip/tilt/focus modes that cannot be obtained from the LGSs. We based our simulations on MIRAO, an AO system that aims to have low thermal emissivity while providing corrections in the mid-IR wavelengths. The current design calls for three LGSs and a single NGS used for tip/tilt/focus sensing. The system has a 60×60 subaperture array with a single deformable mirror operating at 800 Hz.

Even with an Alluxa OD4 filter and a threshold subtracting the background from each frame, the residual noise proved too large for stable operation of the AO system. As such, a configuration was chosen to boost the SNR for the LGS WFS with the Alluxa OD4 filter to a point we were certain the AO system would be stable. We chose a SNR value of 20 with the expectation that it would be robust to variations in the sky background. To keep the results in-line with the performance of the Alluxa OD4 filter, we instead tuned the design of the AO system. In the background limited case, our SNR value is approximated by

$$\text{SNR} \approx \frac{S}{\sqrt{B}} = \frac{\eta D^2_{\text{subap}} t T_{589} 900}{\sqrt{\eta D^2_{\text{subap}} t \Delta\lambda \Omega_{\text{FoV}} F_{\text{sky}}}} \propto \frac{\sqrt{\eta t} D_{\text{subap}}}{\sqrt{\Omega_{\text{FoV}}}}. \quad (2)$$

By using the NFIRAOS WFS design, we have already optimized Ω_{FoV} to minimize sky background while still capturing the fully elongated LGS spot. From the remaining parameters, we decided to change the subaperture collecting area, since the other parameters go as their square root. To reach an SNR of 20, we needed a factor of 3 in subaperture area resulting in a 34×34 subaperture array.

Importantly, this configuration is still achievable with the base MIRAO design through two possibilities. First, swappable lenslet arrays have been implemented in other systems (e.g., PALM-3000[16]). However, the filter has additional angle of incidence limitations (see Sec. 4.2) that may complicate such a design. Second, one could bin together 2×2 sets of subapertures by averaging the measurement of each one. Since the measurements are background limited, this does not add additional noise compared to the case of using a single subaperture that is 4 times as large. Binning this way would create the equivalent of a 30×30 array, roughly the same as what we have simulated.

Recent discussions among the MIRAO team have indicated a desire to boost the performance of the system at shorter wavelengths. To address this possibility, we also added two LGSs in order to reduce the LGS focal-anisoplanatism. This also helps the NGS WFS, which operates in the K-band. It is important to note that the additional LGSs have no impact on whether or not this system can run during the day, and this change is meant only to reflect the potential changes to the MIRAO design. For all of the simulations presented here we assume that the science object is also used as the NGS. These changes led to stable operation of the system, and so the final configuration is a 5 LGS, 1 NGS system with 34×34 subapertures running at 800 Hz on a single deformable mirror.

For the NGS WFS, we chose K-band (i.e., 2.2 μm) to benefit from the AO corrected point spread function and from a lower sky background. However, we did not perform an optimization here and shorter or longer wavelengths could be considered. Our simulations used K-band sky brightness values measured using the near-IR guider camera of the iShell instrument on IRTF. Observations of the star HD377 were made in clear conditions. This was done at 07:42 AM local time with the star ~90 deg away from the Sun. The result of these measurements can be found in Table 2 along with the other sky brightness measurements.

The performance of the AO system demonstrated in Fig. 4 reflects that of a robust (see Sec. 4.1) daytime system, which achieves near optimal (i.e., nighttime) performance down to NGS magnitudes of $K \sim 13$. Table 4 contains a list of attainable Strehl ratios at longer wavelengths. For brighter NGS magnitudes, the performance is driven by the LGS component of
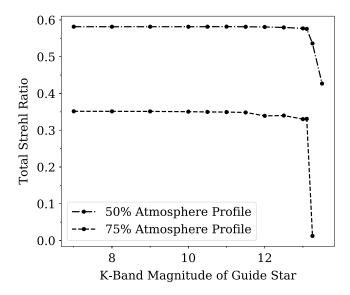
Fig. 4 The total K-band Strehl ratio versus magnitude of the NGS for the MIRAO system (see Sec. 3.2) in daytime conditions. The sky background for the NGS (tip, tilt, focus) WFS corresponds to our measured MKO K magnitude value. The sky background for the LGS WFS corresponds to the expected flux through the Alluxa OD4 filter. The sharp decrease in performance at the $K \sim 13$ results from the rapid decrease in the SNR of the NGS WFS against the day time sky.

Table 4 Strehl ratio at science wavelengths of interest.

Wavelength (μm)	Total Strehl ratio (%)
2.2	58
3.8	83
4.7	89
10.8	98
13.0	99

the system since the reduction in the Strehl ratio from the corrected low order aberrations is less than 1%. For fainter NGSs, there is a sharp drop in performance. This sharp drop is partially from the fact that the NGS WFS parameters were not optimized for fainter guide star magnitudes. However, even with an optimization, we expect the limiting magnitude cut-off to be sharper than that for a nighttime system. To see why, consider a nighttime SHWFS for which the sensitivity is often limited by read noise so the SNR can improve proportionally with increasing the WFS integration time ($SNR \sim t$). However, for the daytime case, the system is background limited so the SNR increases only as $\sim \sqrt{t}$. Since this study is concerned with demonstrating the feasibility, system parameters were not optimized as a function of guide star brightness. Doing so should extend the limiting magnitude of the system fainter.

4 Discussion

Our calculations indicate that a relatively simple, inexpensive, interference filter can enable daytime AO with a sodium LGS. In this section, we comment on the sensitivity of our approach to variations in the sky brightness and discuss some important design constraints imposed by the interference filter approach for LGSs.

4.1 Sky Brightness Variations

Throughout this paper, we have assumed a sky brightness based on a single measurement taken with an observing angle 90 deg away from the Sun, which corresponds to the darkest part of the sky. A major objection to this approach would be that the sky brightness will vary with observing angles relative the Sun (look angles), with time of day, with day-to-day variations in aerosol content of the atmosphere, and over the course of a year. We could not find a long-term survey of the daytime sky brightness in the near-infrared or visible bands. However, models of atmospheric scattering processes have been used to explore how near-IR sky brightness varies with time of day, look angle, and by time of year for Haleakala.[17] Moreover, observations for this site have since proven consistent with these predictions.[18] If we apply the expected restrictions for a large night-time astronomical telescope, limiting observations to the first few hours of the morning and to look angles between 90 and 120 deg (e.g., ~2 h of observing a target), then the sky variation is only about one magnitude. To address this, we first computed the expected SNR of our Alluxa OD4 filter over a range of sky brightness values [see Fig. 5(a)]. We then ran simulations covering the full range of resulting SNR values that we had calculated. The plotted data [Fig. 5(b)] demonstrate how the system would perform over a wide range of SNR values and, by extension, sky brightnesses. As expected, increasing the sky background degrades the performance of the AO system. Additionally, we find that an SNR of 12 appears to be the lower limit of this system, which corresponds to a sky, which is three times brighter than our measured value (i.e., over one magnitude brighter). The lower limit comes from the point at which the simulations are too unstable to finish a full set of 20 simulation runs.

There are a few other features worth highlighting in Fig. 5. First, the point with the highest SNR in Fig. 5 corresponds to the night time sky performance (i.e., $B = 0$), so it represents the optimal performance of this system. Second, that the performance levels off with increasing SNR, lending credence to the idea that the narrowest possible bandpass is not a requirement for a daytime AO system. For the configuration described in Sec. 3, we find that the performance of the Alluxa OD4 filter is robust for sky brightness changes as large as at least one magnitude. We note that an allowance for sky surface brightness variations should be accommodated in the design of the system and that some characterization of the sky brightness at the telescope site would be useful input to the design.

As mentioned in Sec. 2.3, the filter profile was measured to be wider than that which the manufacturer provided for us. While the simulations used the filter profile provided to us by the vendor and not the one we measured, our conclusions remain unchanged. The reason for this lies in our sensitivity to sky brightness variations. Calculating the expected SNR of the measured filter profile yields a value of 16, which still falls within our operable range, as demonstrated in Fig. 5. The increase in filter bandpass is roughly the equivalent of the sky increasing in brightness by a factor of 2. This does reduce the flexibility of our system's configuration with respect to variations that lead to a brighter sky; however, with an improved bandpass for the interference filter, we can regain this flexibility.
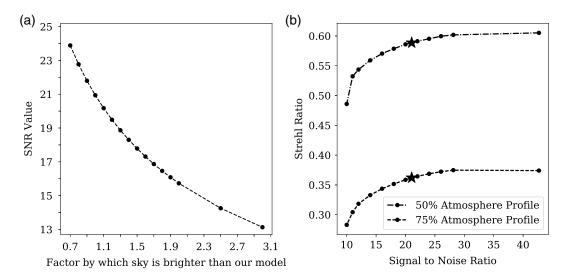
Fig. 5 (a) A plot of the expected SNR of the Alluxa OD4 filter that was chosen in Sec. 2 versus the sky brightness. The sky brightness is expressed as a multiplicative factor relative to our measured value. For example, a factor of 2 represents two times as many background photons measured by the WFS. (b) The high order (tip/tilt/piston removed) K-band Strehl ratios for the MIRAO system in both the 50th and 75th percentile atmosphere cases (median and poor seeing respectively) versus SNR achieved in the WFS. The SNR is calculated according to Eq. (1) with $T_{589} = 0.9$ and $A = 3$. The star on each curve reflects the expected performance of the Alluxa OD4 filter (SNR of 21) for our modeled sky brightness.

4.2 Optical Layout Considerations

There are also optical design constraints that need to be considered. First, since the sky is such a dominant background source, a field stop at the entrance of the WFS is required to keep the sky background low in each subaperture. This is especially true for a SHWFS, where each subaperture has the potential of seeing the sky from all adjacent subapertures. Second, the variation of the central wavelength of the filter as a function of angle of incidence sets a field size limitation. For MIRAO, the filter needs to pass a FoV of about 4 to 6 arc sec to accommodate the elongation of the laser spot as seen by subapertures near the edge of the pupil. For TMT with a laser launched from behind the telescope secondary mirror (i.e., on-axis), the elongated spots in the subapertures near the edge of the pupil are expected to be 3 to 4 arc sec in length. Assuming the filter is placed at a pupil position in the WFS, this angular size on the sky is magnified by the pupil magnification at the filter location. For a TMT and a 30-mm pupil size, this is a factor of 1000. The subaperture image would be attenuated by 85% at ±2 arc sec. One can create a larger pupil size and use a larger interference filter but this increases the size and cost of the instrument. Alternatively, one can increase the filter bandpass and compensate for the increased sky background by increasing the size of the subapertures (reducing the overall AO performance). Finally, one could accept some attenuation of the LGS spot at the edges of the field. We have not studied the impact of this on the performance of the system and will leave it to a future study. However, we note that most of the flux will be contained within the center ~3 to 4 arc sec, whereas the attenuation is in the tails of the LGS image. Each of these considerations has their own respective trade-offs, which will need to be considered when designing a sodium LGS AO system to be used during the day.

4.3 Temperature Variations

Another important consideration is the temperature of the interference filter, as the central wavelength will vary with the environmental temperature. The wavelength change is proportional to the temperature change with a proportionality constant of 0.01 to 0.03 nm/°C. An increase in temperature increases the central wavelength. Thus, for a 10°C increase in temperature, the central wavelength shifts by about 0.3 nm, more than half of the bandpass of the Alluxa OD4 filter. One can compensate for this with a small tilt of the filter with respect to the incoming beam. For example, a tilt of about 2 deg would compensate for this shift in the Alluxa OD4. In practice, we could consider designing filters for a lower range of temperatures and then tilting them to compensate for variations due to higher temperatures. If instead we wanted to limit the amount of tilt compensation, we could implement a set of filters all designed for slightly different base temperatures. Such an approach is feasible given the low cost of the interference filters.

5 Conclusion

Our study indicates that a sodium LGS based AO system can work in daytime conditions with an off-the-shelf narrow-band-pass interference filter and a K-band NGS WFS for tip/tilt/focus sensing. The key filter requirements are a bandpass less than 500 pm, a flat top response with a high (greater than 90%) throughput at the central wavelength of the LGS return, and an out-of-band suppression of at least OD 4. The size of the WFS subapertures and the brightness of the LGS needs to be large enough to overcome the still higher sky background. Simulations of a system like MIRAO for TMT show that a system with 34×34 subapertures, five LGSs, and a single on-axis NGS for tip/tilt/focus sensing can deliver Strehl ratios greater than 80% throughout the thermal infrared range during the day when there is a NGS with K magnitude greater than 13.

The limiting magnitude of the system is determined by the NGS used for tip/tilt/focus correction.

Fine tuning of the filter specifications, the order of the AO system, and optimization of the system control parameters can potentially yield higher Strehl ratio values and fainter limiting magnitudes. However, this optimization needs to be done in the context of knowledge of the variations of the sky brightness and an operational plan for the daytime observing. These will be explored in a future study.

This work also has implications for existing LGS AO systems. The ability to operate a sodium LGS in daytime conditions opens up the early twilight hours for system calibrations. This frees up time during the night normally spent setting up and calibrating the system. For some systems, this can amount from 20 to 30 min of additional science time per night.[19] Additionally, this could extend the time available for observations in the near-infrared wavelengths.

Acknowledgments

References

1. J. Beckers and A. Cacciani, "Using laser beacons for daytime adaptive optics," *Exp. Astron.* **11**(2), 133–143 (2001).
2. G. Herriot et al., "NFIRAOS: first facility AO system for the Thirty Meter Telescope," *Proc. SPIE* **9148**, 914810 (2014).
3. C. Boyer et al., "Adaptive optics program at TMT," *Proc. SPIE* **9148**, 91480X (2014).
4. J. M. Beckers, "Laser guide stars for daytime thermal IR observations," *Proc. SPIE* **6986**, 69860G (2008).
5. M. Hart, S. M. Jefferies, and N. Murphy, "Daylight operation of a sodium laser guide star for adaptive optics wavefront sensing," *J. Astron. Telesc. Instrum. Syst.* **2**, 040501 (2016).
6. J. W. Hardy, *Adaptive Optics for Astronomical Telescopes*, Oxford University Press, New York (1998).
7. C. Boyer et al., "The TMT laser guide star facility," in *Adapt. Opti. Extremely Large Telescope*, p 04004 (2010).
8. B. Ellerbroek et al., "The TMT adaptive optics program," in *Second Int. Conf. Adaptive Optics Extremely Large Telescope*, p. 6 (2011).
9. J. Lyke and R. Campbell, "LGSAO basics and system description," 2016, https://www2.keck.hawaii.edu/optics/lgsao/lgsbasics.html (22 June 2017).
10. K. Chance and R. L. Kurucz, "An improved high-resolution solar reference spectrum for earth's atmosphere measurements in the ultraviolet, visible, and near infrared," *J. Quant. Spectrosc. Radiat. Transfer* **111**, 1289–1295 (2010).
11. A. A. S. Gulbis et al., "First results from the MIT Optical Rapid Imaging System (MORIS) on the IRTF: a stellar occultation by Pluto and a transit by Exoplanet XO-2b," *Publ. Astron. Soc. Pac.* **123**, 461–469 (2011).
12. Alluxa, Private Communication, Alluxa Incorporated, California (2018).
13. W. Lianqi and B. Ellerbroek, "Fast end-to-end multi-conjugate AO simulations using graphical processing units and the MAOS simulation code," in *Second Int. Conf. Adaptive Optics Extremely Large Telescope*, p. 5 (2011).
14. M. Schöck et al., "Thirty meter telescope site testing I: overview," *Publ. Astron. Soc. Pac.* **121**, 384–395 (2009).
15. E. S. Bradley et al., "Characterization of meteorological and seeing conditions at Haleakala," *Publ. Astron. Soc. Pac.* **118**(839), 172–182 (2006).
16. J. E. Roberts et al., "Results from the PALM-3000 high-order adaptive optics system," *Proc. SPIE* **8447**, 84470Y (2012).
17. K. Jim, B. Gibson, and E. Pier, "Daytime sky brightness modeling of Haleakala along the GEO belt," in *Advanced Maui Optical and Space Surveillance Technologies Conf.*, p. 68 (2012).
18. M. Hart et al., "Quantitative measurements of the daytime near infrared sky brightness at the AEOS 3.6 m telescope," in *Advanced Maui Optical Space Surveillance Technologies Conf.*, p. E73 (2014).
19. P. Wizinowich, Private Communication (2017).

Ryan Dungee is a graduate student at the University of Hawaii. He received his BA and MS degrees in physics from the University of Pennsylvania in 2015 and 2016, respectively. He is working on a PhD in astronomy currently. His current research interests are ground layer adaptive optics, astrochemistry, and young stellar objects.

Mark Chun is an associate specialist at the Institute for Astronomy at the University of Hawaii-Manoa. He received his PhD degree in astronomy and astrophysics from the University of Chicago in 1997. He has worked on the deployment of five adaptive optics systems on telescopes around the world. His current research interests include extending adaptive optics corrections to very wide fields of view and novel wavefront sensing approaches.

Yutaka Hayano is an associate professor at National Astronomical Observatory of Japan. He received his PhD degree in astronomy from the University of Tokyo in 1995. He has worked on the laser guide star adaptive optics system for Subaru Telescope and ground-to-satellite laser communication. He is currently working for the first generation instrument, IRIS, for TMT. His current research interests are expanding the applications and technologies of adaptive optics.